Available online at www.sciencedirect.com
SCIENCE DIRECT®
Journal of Sound and Vibration 285 (2005) 783–801
JOURNAL OF SOUND AND VIBRATION
www.elsevier.com/locate/jsvi

Optimal spatial sampling interval for damage detection by curvature or strain energy mode shapes

Edward Sazonov[a,*], Powsiri Klinkhachorn[b]

[a]*Department of Electrical and Computer Engineering, Clarkson University, P.O. Box 5720, Potsdam, NY 13699, USA*
[b]*Lane Department of Computer Science and Electrical Engineering, Morgantown, WV 26506, USA*

Received 17 November 2003; received in revised form 23 July 2004; accepted 27 August 2004
Available online 21 December 2004

Abstract

Vibration-based methods of non-destructive damage detection utilizing curvature or strain energy mode shapes have been applied in a variety of applications. Attractive features of these methods include high sensitivity to damage and instant determination of the damage location. However, the quality of damage detection achieved in practice depends upon determining a proper sampling interval for discretization of the displacement mode shapes. Experimental observations show that both undersampling and oversampling of the displacement mode shapes may have adverse effects on the quality of damage detection. This paper presents an analysis aimed at determining the optimal sampling interval that would minimize the effects of measurement noise and truncation errors on the calculation of the curvature and strain energy mode shapes, thus maximizing sensitivity to damage and accuracy of damage localization. Derivation of the formulas for the optimal sampling interval is based on the most commonly used numerical methods for the computation of the curvature and the strain energy mode shapes. Numerical verification has shown very good performance of the suggested formulas in predicting the optimal sampling interval.

1. Introduction

Damage detection by curvature or strain energy mode shapes has been widely discussed in research literature and used in practical applications. These methods not only allow

*Corresponding author. Tel.: +1 315 268 3914; fax: +1 315 268 7600.
E-mail address: esazonov@clarkson.edu (E. Sazonov).

0022-460X/$ - see front matter © 2004 Elsevier Ltd. All rights reserved.
doi:10.1016/j.jsv.2004.08.021

detection of damage in a structure but also determination of damage location with high degree of accuracy.

Pandey et al. [1] detected location of cracks by observing changes in curvature mode shapes. The authors showed that damage introduced into the structure led to local changes in the shape of curvature mode shapes and could be observed by comparing curvature mode shapes of the damaged structure to the curvature mode shapes of the undamaged structure. Ratcliffe [2], and Hoerst and Ratcliffe [3] introduced a modified Laplacian operator for damage detection using mode shape information. This method had the same numerical formula for computing mode shapes as in Ref. [1]. Farrar and Jauregui [4] conducted a comparative study of different damage identification algorithms on a bridge. The curvature-based methods performed very well compared to other methods tested in the experiments, occupying the top two places of the accuracy of detection. The authors also noted the methods' high sensitivity to less severe damage cases. Lu et al. [5] used flexibility curvature in simulated experiments on the reinforced concrete beams. Sampaio [6] described a frequency response function curvature method, based on Pandey's work. Dutta and Talukdar [7] considered using curvature mode shapes for better localization of damage in bridges.

Several variations of the strain energy method have been discussed in recent literature. Petro et al. [8] tested the strain energy method on aluminum beams, trying to establish the method's applicability to damage detection in an aluminum portable bridge. Venkatappa [9] described a variation of the strain energy mode shapes method used in the analysis presented in this paper. The damage detection procedure was based on comparing the strain energy mode shapes for the damaged structure to those of the undamaged structure. The author reported that the strain energy method had shown more sensitivity to damage than other mode shape-based methods. Osegueda et al. [10] investigated the strain energy method on aluminum cantilever beams and honeycomb composite plates. The authors received positive damage detection results in experiments with beams and negative results in experiments with composite plates. They also reported that strain energy methods not only can identify damage but also quantify it by accounting the energy relations between damaged and undamaged states. In another work of Carrasco et al. [11], the authors applied the strain energy method to damage detection in a space truss model. The reported results were partially successful. The method detected more severe damage cases, while some of the less severe cases went undetected. Cornwell et al. [12] performed a comparative study of two vibration-based damage identification algorithms, including the strain energy method. The testing was conducted on a beam and a plate, comparing the damaged vs. undamaged strain energy distribution. The strain energy method successfully identified severe damage cases, but a masking effect was reported for lower level damages, i.e., when the two damage locations had different levels of damage, the algorithm tended to only conclusively identify the location with the largest amount of damage. Wahab and Roeck [13] used modal curvatures to detect damage in bridges by using the change in dynamic parameters between the intact and damage states. The experiments were conducted on a prestressed concrete bridge. This paper also introduced a damage indicator called "curvature damage factor", in which the difference in curvature mode shapes for all modes can be summarized in one number for each measurement point. Yoo et al. [14] used the difference in strain energy mode shapes between damaged and undamaged cases to detect and locate damage in a plate. Pereyra et al. [15] studied damage detection in an aluminum stiffened-plate panel resembling aircraft fuselage construction.

As in most other studies, the damaged strain energy mode shapes were compared to the undamaged strain energy mode shapes. Statistical methods were employed to jointly analyze information from several mode shapes and to locate damage. Cornwell et al. [16] provided a detailed theoretical explanation on application of the strain energy method to plate-like structures. They reported that the method was effective enough to detect areas with10% reduction in stiffness. Ndambi et al. [17] utilized strain energy mode shapes for damage assessment in reinforced concrete beams. Kim et al. [18] conducted comparative studies of frequency-based and a mode-shape-based methods. The mode-shape-based method utilized computations of the modal strain energy and provided higher accuracy of damage localization than the frequency-based method.

A few recent studies have addressed the issue of determining the proper sampling interval for acquisition of the displacement mode shapes that could be utilized in strain energy or curvature calculations. Napolitano [19] investigated the quality of damage detection using reduced measurements and the strain energy algorithm. The work featured a finite element model of a free–free beam sampled with the number of sampling points varying from 11 to 101. The author concluded that the strain energy method performs better when many response points are measured. Shi and Law [20] investigated damage localization from modal strain energy change in simulated experiments. The authors considered the effects of measurement noise and systematic errors by artificially adding random noise to the simulation results. They noted that measurement noise and incompleteness of measured modes greatly affect the result of damage localization. Yoo and Kim [21] tried to experimentally establish the minimal number of sensing elements in a grid covering the plate to identify the damage location with sufficient accuracy. Yan and Deng [22] applied the strain energy algorithm to non-destructive damage detection in bridges. They conducted numerical experiments on a finite element model of a freely supported bridge T-beam. Among the conclusions made in the paper, one is that "the key of damage detection of real bridges using strain energy is the measurement accuracy of the vibration amplitude".

In most works covering damage detection by curvature or strain energy mode shapes, the utilized sampling interval has been set intuitively. The spatial resolution (number of sampling points) used to acquire displacement mode shapes (reciprocal of the sampling interval) was chosen to be that at a level that seems to be suitable but has no firm justification. Conclusions reached by many authors studying effects of the spatial resolution on the damage detection results follow the intuitively reasonable path: the more the sampling points, the better. This is a completely valid approach for acquisition of the displacement mode shapes (direct consequence of the Nyquist's sampling theorem), but it cannot be automatically extended to curvature or strain energy mode shapes. Indeed, accuracy of locating the damage directly depends on the sampling interval. Lower sampling interval allows localizing the damage with higher precision. At the same time, practical application of the curvature and strain energy mode shapes is subject to the effects of measurement noise, which may render "the more the better" approach invalid. Modern instrumentation, such as laser doppler vibrometers (LDV), allow for very high density of sampling and high precision of acquiring the mode shapes. Ideally, the accuracy of localizing the damage should be proportional to the decrease in the sampling interval. Practice, however, disproves this hypothesis.

To demonstrate this point, Fig. 1 shows strain energy mode shapes computed from the data acquired by an Ometron VPI-4000 laser vibrometer on a free–free aluminum beam (4th bending

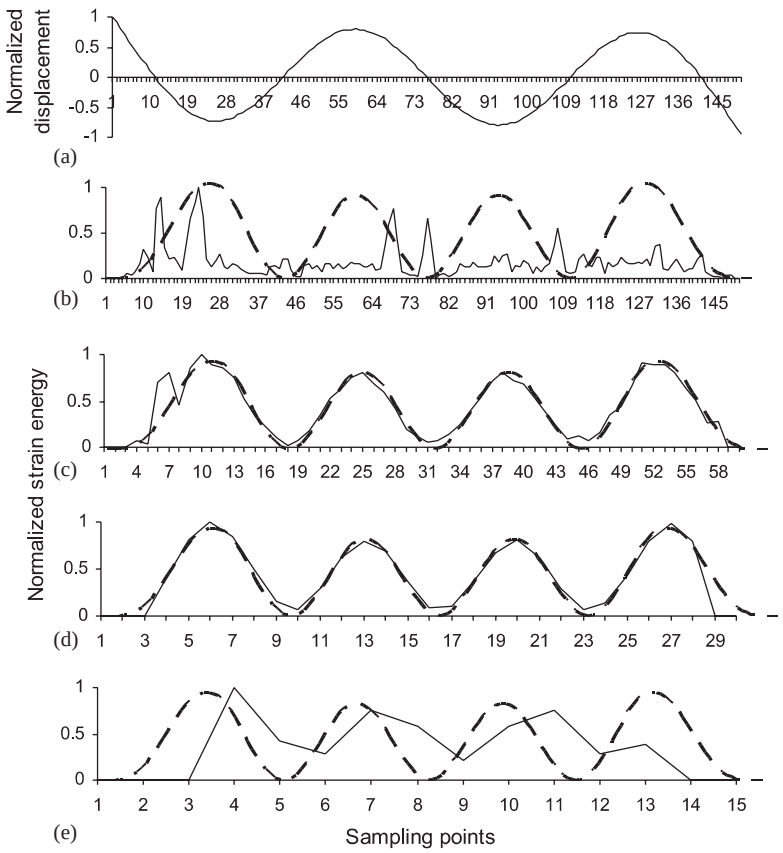

Fig. 1. Fourth bending mode shape of an undamaged free–free beam: (a) ideal (dashed line) and computed (solid line) strain energy mode shapes for the fourth bending mode shape of an undamaged free–free beam; (b) 150 sampling points; (c) 60 sampling points; (d) 30 sampling points; (e) 15 sampling points.

mode shape). Clearly, both the strain energy mode shape computed with just a few points (15 points) and the strain energy mode shape computed on too many points (150 points) are not suitable for damage detection due to severe distortion in the shape of the computed strain energy mode shapes. The strain energy mode shape computed on 30 points provides the best approximation of the actual mode shape with the least amount of false peaks by utilizing a near-optimal sampling interval. The answer to determining the optimal sampling interval for strain energy and curvature mode shapes seems to be in the connection between the measurement noise and the numerical properties of the computational methods used to calculate the curvature and strain energy mode shapes. This paper provides both analytical and numerical justification for the selection of the proper sampling interval for performing damage detection on curvature and strain energy mode shapes with the most commonly used numerical methods. The analysis is performed for the errors originating as the effects of measurement noise and does not consider the errors in the spatial interval itself. Practically applicable formulas are supplied as a result of the research.

2. Analysis of curvature mode shapes

Computation of the curvature mode shapes is an integral part of the strain energy method. Calculations of curvature mode shapes are always performed before the strain energy mode shapes can be computed. Thus, it is convenient to start the study of the numerical properties of the strain energy mode shapes with the study of curvature mode shapes and then extend the results to strain energy mode shapes.

The method of curvature mode shapes is described in Ref. [1]. The authors showed that damage introduced into the structure led to local changes in the shape of curvature mode shapes and could be observed by comparing curvature mode shapes of the damaged structure to the curvature mode shapes of the undamaged structure. Computation of the curvature mode shapes from displacement mode shapes is usually performed using the central difference second derivative formula [1]:

$$\varphi''(x) = \frac{\varphi(x+h) - 2\varphi(x) + \varphi(x-h)}{h^2}, \tag{1}$$

where φ is the displacement mode shape sampled with the sampling interval h.

It is a known fact that computation of numerical derivatives using finite differences is very prone to noise in the data for smaller sampling intervals (more sampling points) [23]. At the same time, larger sampling intervals (less sampling points) may cause imperfect restoration of the curvature mode shapes due to the truncation error [24]. Therefore, proper spatial resolution n (the reciprocal of the sampling interval h) for sampling of displacement mode shapes should be high enough to avoid truncation error and, at the same time, low enough to avoid errors due to the perturbation in the data. The error in the curvature mode shapes computed by formula (1) can be estimated as follows.

Denote $\varphi_1 = \varphi(x_0 + h)$, $\varphi_0 = \varphi(x_0)$, $\varphi_{-1} = \varphi(x_0 - h)$; then the value of a curvature mode shape computed from φ at the location x_0 is [24]

$$\varphi''(x_0) = \frac{\varphi_1 - 2\varphi_0 + \varphi_{-1}}{h^2} + e_2, \quad e_2 = -\frac{h^2}{12}\varphi^{IV}(\xi), \tag{2}$$

where e_2 is the approximation error of $O(h^2)$.

In practice, the exact values of φ_1, φ_0 and φ_{-1} are not known. Assume that the measurement device generates an absolute constant additive error α and a relative multiplicative error ε. Then the values of φ acquired from the measurement equipment are

$$\bar{\varphi}_1 = \varphi_1 + \alpha + \varepsilon_1\varphi_1, \quad \bar{\varphi}_0 = \varphi_0 + \alpha + \varepsilon_0\varphi_0, \quad \bar{\varphi}_{-1} = \varphi_{-1} + \alpha + \varepsilon_{-1}\varphi_{-1}, \quad |\varepsilon_{\pm 1}| \leqslant \varepsilon. \tag{3}$$

Formula (2) becomes

$$\varphi''(x_0) = \frac{\bar{\varphi}_1 - 2\bar{\varphi}_0 + \bar{\varphi}_{-1}}{h^2} - \frac{\varepsilon_1\varphi_1 - 2\varepsilon_0\varphi_0 + \varepsilon_{-1}\varphi_{-1}}{h^2} + e_2. \tag{4}$$

The term $(\bar{\varphi}_1 - 2\bar{\varphi}_0 + \bar{\varphi}_{-1})/h^2$ is what actually is being computed during the curvature mode shape calculations. The corresponding error is

$$E_2 = \varphi''(x_0) - \frac{\bar{\varphi}_1 - 2\bar{\varphi}_0 + \bar{\varphi}_{-1}}{h^2} = -\frac{\varepsilon_1\varphi_1 - 2\varepsilon_0\varphi_0 + \varepsilon_{-1}\varphi_{-1}}{h^2} + e_2. \tag{5}$$

The maximum bound on the error can be estimated as

$$|E_2| \leqslant \frac{\varepsilon(|\varphi_1| + 2|\varphi_0| + |\varphi_{-1}|)}{h^2} + \frac{M_4}{12} h^2 \tag{6}$$

where $M_4 = \max_{([x_0-h, x_0+h])}|\varphi^{IV}(x)|$.

In Eq. (6), the term $\varepsilon(|\varphi_1| + 2|\varphi_0| + |\varphi_{-1}|)/h^2$ corresponds to the error due to the noise in data, and the term $(M_4/12)h^2$ corresponds to the truncation error introduced by replacing the derivative by a finite difference expression. Denoting the bound on the right of Eq. (6) as

$$E(h) = \frac{\varepsilon(|\varphi_1| + 2|\varphi_0| + |\varphi_{-1}|)}{h^2} + \frac{M_4}{12} h^2, \tag{7}$$

the optimal sampling interval h_0 can be determined by finding the minimum of $E(h)$:

$$E(h) \geqslant E(h_0), \quad h_0 = \sqrt[4]{\frac{\varepsilon(12|\varphi_1| + 24|\varphi_0| + 12|\varphi_{-1}|)}{M_4}} = \sqrt[4]{\varepsilon F_4}, \tag{8a}$$

where $F_4 = (12|\varphi_1| + 24|\varphi_0| + 12|\varphi_{-1}|)/M_4$ for $x = x_0,\ x_0 \in (0, L)$; L is the length of a curvature mode shape. Eq. (8a) produces the optimal sampling interval for sampling in the neighborhood of x_0. Note that though in general $x_0 \in (0, L)$, the results are only valid when $x_0 - h \geqslant 0$ and $x_0 + h \leqslant L$. To determine the optimal sampling interval for sampling a displacement mode shape on a beam of a finite length L and subsequent computing of a curvature mode shape, the worst case value of F_4 should be determined on the interval $(0, L)$ and used in formula (8a):

$$h_0 = \sqrt[4]{\varepsilon F_4}, \quad F_4 = \max_{[0,L]}\left(\frac{(12|\varphi_1| + 24|\varphi_0| + 12|\varphi_{-1}|)}{M_4}\right) \quad \text{for } \forall x \in (0, L). \tag{8b}$$

Formula (8b) was obtained by assuming that the value of F_4 is a constant and is independent of h. Although not true in general, such an assumption is valid because F_4 can be estimated numerically, thus establishing the maximum values that can be used for practical calculations.

For example, the displacement mode shape equation for the most commonly used free–free beam [25] for the mode k is

$$\Phi_k(x) = \cosh\left(\frac{\lambda_k x}{L}\right) + \cos\left(\frac{\lambda_k x}{L}\right) - \sigma_k\left(\sinh\left(\frac{\lambda_k x}{L}\right) + \sin\left(\frac{\lambda_k x}{L}\right)\right), \tag{9}$$

where L is the length of the beam, λ_k and σ_k are mode shape coefficients dependent on k: $\lambda_k = \{4.730040739999998, 7.853204619999998, 10.9956078, 14.1371655, 17.27875969999999, (2k+1)\pi/2 \text{ for } k > 5\}$; $\sigma_k = (\cosh\lambda_k - \cos\lambda_k)/(\sinh\lambda_k - \sin\lambda_k)$

The fourth derivative of Eq. (9) with respect to x is

$$\Phi_k^{IV}(x) = \frac{\lambda_k^4 \cosh(\lambda_k x/L)}{L^4} + \frac{\lambda_k^4 \cos(\lambda_k x/L)}{L^4} - \sigma_k\left(\frac{\lambda_k^4 \sinh(\lambda_k x/L)}{L^4} + \frac{\lambda_k^4 \sin(\lambda_k x/L)}{L^4}\right). \tag{10}$$

Both Eqs. (9) and (10) can be discretized for a number of sampling intervals h and used to estimate F_4 for different values of h and k. Fig. 2 shows the graphs of F_4 for the first bending mode ($k = 1$) of a free–free beam with the length $L = 1$ sampled with $n = 1/h = 30$ and $n = 300$. The maximum value of F_4 for $n = 30$ is 0.09505 and for $n = 300$ is 0.09588. Fig. 3 shows the

graphs with the same parameters for the second bending mode ($k = 2$) of a free–free beam. The maximum values of F_4 are 0.01236 ($n = 30$) and 0.01261 ($n = 300$).

Figs. 2 and 3 show that the maximum value of F_4 has very little dependency on the sampling interval h, but it is significantly different for different modes k, decreasing in value as k grows. Thus, a larger number of sampling points n (smaller sampling interval h) can be used for the higher order modes acquired with the same measurement noise level ε as the lower order modes. For practical calculation of h_0, the maximum of F_4 can be numerically estimated for a sufficiently high n, such as $n = 300$.

Table 1 shows values of F_4 for the first five bending modes of beams with different boundary conditions and unit length $L = 1$, computed with $n = 300$. Values supplied in the table should be used directly in formula (8b) to obtain the optimal sampling interval for a displacement mode shape. The values of h_0 computed from Eq. (8b) should be adjusted for the actual length of a beam ($h_{0L} = h_0 L$) or used to compute the optimal spatial resolution $n_0 = 1/h_0$. The same is true for the formulas derived later in this paper.

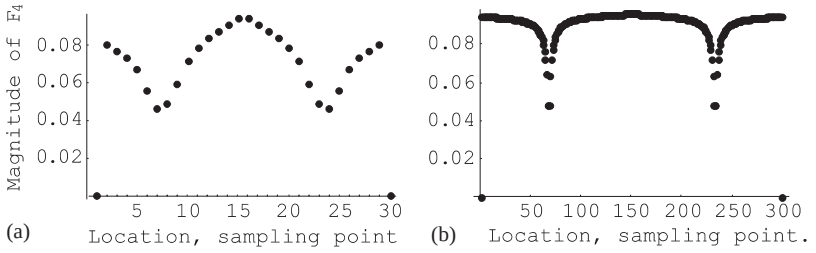

Fig. 2. Numerical estimate of F_4 for the first mode of a free–free beam: (a) $n = 30, L = 1$; (b) $n = 300, L = 1$.

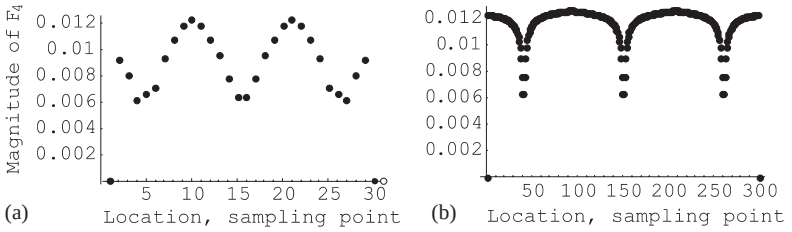

Fig. 3. Numerical estimate of F_4 for the second mode of a free–free beam: (a) $n = 30, L = 1$; (b) $n = 300, L = 1$.

Table 1
Numerical estimates of F_4 for different boundary conditions

Boundary conditions	Mode 1	Mode 2	Mode 3	Mode 4	Mode 5
Free–free, clamped–clamped	0.09588	0.01261	0.003282	0.001201	0.000538
Pinned–pinned, sliding–sliding	0.4927	0.0307	0.006082	0.001924	0.000788
Clamped–pinned	0.2019	0.01922	0.004415	0.001509	0.000648
Clamped–free	3.864	0.09885	0.0126	0.003282	0.001201

Formula (8b) establishes the optimal sampling interval that minimizes the maximum absolute error in calculations of the curvature mode shapes and also minimizes the effect of the measurement noise. The same formula can be used both for damaged and undamaged beams because changes in the displacement mode shapes due to damage are usually minimal and can be neglected. An interesting observation following from Eq. (8b) is that doubling the spatial resolution (sampling a displacement mode shape at twice the number of sampling points) requires decreasing the measurement noise by a factor of 16!

Another point of interest would be the value of the sampling interval h_m at which the maximum computational error becomes equal to or greater than the maximum value of $\varphi''(x)$. Acquiring a displacement mode shape with $h \geqslant h_m$ will lead to amplification of the measurement noise, rather than computation of $\varphi''(x)$.

Establishing h_m requires solving the equation

$$\frac{\varepsilon(|\varphi_1| + 2|\varphi_0| + |\varphi_{-1}|)}{h^2} + \frac{M_4}{12} h^2 = \max_{[0,L]} |\varphi''(x)|. \tag{11}$$

The analytical solution of Eq. (11) can be obtained as follows. Denote $M_{2L} = \max_{[0,L]}|\varphi''(x)|$. Then, after multiplying both parts by $12h^2/M_4$, Eq. (11) becomes

$$\frac{12\varepsilon(|\varphi_1| + 2|\varphi_0| + |\varphi_{-1}|)}{M_4} + h^4 - \frac{12M_{2L}h^2}{M_4} = 0 \quad \text{or}$$

$$\varepsilon F_4 + h^4 - \alpha h^2 = 0, \quad \text{where} \quad \alpha = 12M_{2L}/M_4. \tag{12}$$

Solution of Eq. (12) gives

$$h_{m\text{LOW}} = \sqrt{\frac{\alpha}{2} - 0.5\sqrt{\alpha^2 - 4\varepsilon F_4}} \quad \text{and} \quad h_{m\text{HIGH}} = \sqrt{\frac{\alpha}{2} + 0.5\sqrt{\alpha^2 - 4\varepsilon F_4}}. \tag{13}$$

The root $h_{m\text{LOW}}$ corresponds to the error from the measurement noise and the root $h_{m\text{HIGH}}$ corresponds to the truncation error. Only $h_{m\text{LOW}}$ is of interest, due to the fact that there usually is no reason to discretize a function with a sampling interval above h_0. The $h_{m\text{LOW}}$ will further be referred to as h_m:

$$h_m = \sqrt{\frac{\alpha}{2} - 0.5\sqrt{\alpha^2 - 4\varepsilon F_4}}. \tag{14}$$

Only real values of h_m are meaningful. A complex h_m may appear if the noise level in the data is so high that the error exceeds M_{2L} for any h. As in the case with F_4, appropriate value of α can be found numerically. Figs. 4 and 5 show numerical evaluations of α for the first and second displacement mode shapes of the free–free beam computed with $n = 30$ and 300, $L = 1$. The minimal value of α is of interest, because higher values decrease h, reducing the influence of measurement noise. The worst possible scenario should be considered to provide universal applicability of Eq. (14).

Minimal values of α are 0.429821 and 0.425894 for the first bending mode shape ($n = 30$ and 300, respectively); 0.146828 and 0.146 for the second bending mode shape ($n = 30$ and 300, respectively). Analogous to F_4, the dependency of α on h_i is insignificant, while the dependency on k is well-pronounced. Contrary to the behavior of F_4, the worst case values of α should be obtained from a numerical solution featuring a low but practically applicable spatial resolution n,

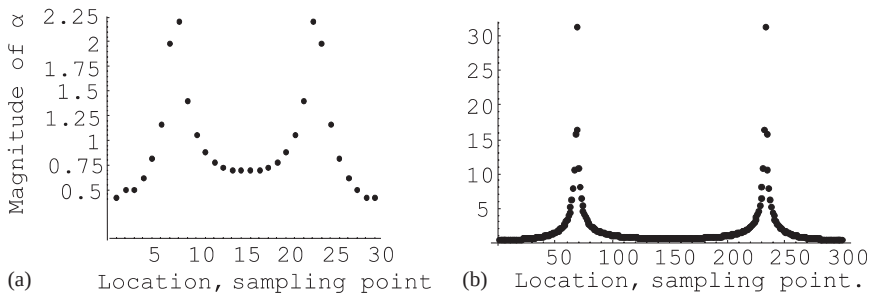

Fig. 4. Numerical estimate of α for the first mode of a free–free beam: (a) $n = 30, L = 1$; (b) $n = 300, L = 1$.

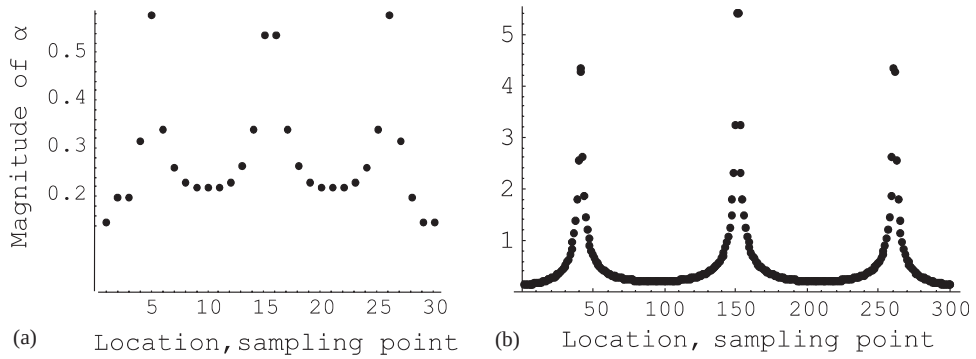

Fig. 5. Numerical estimate of α for the second mode of a free–free beam: (a) $n = 30, L = 1$; (b) $n = 300, L = 1$.

Table 2
Numerical estimates of α for different boundary conditions ($L = 1$)

Boundary conditions	Mode 1	Mode 2	Mode 3	Mode 4	Mode 5
Free–free, clamped–clamped	0.4233	0.1446	0.07482	0.04534	0.02823
Pinned–pinned, sliding–sliding	1.215	0.3039	0.135	0.07599	0.04863
Clamped–pinned	1.031	0.3179	0.1534	0.0902	0.06105
Clamped–free	3.679	0.7275	0.2608	0.1313	0.07949

which was selected to be $n = 20$. Table 2 shows the values of α (for a beam of unit length $L = 1$), that can be utilized in practical calculations of h_m.

Fig. 6 illustrates behavior of the computational error $E(h)$ compared to the behavior of $\varphi''(x)$ computed noise-free through formula (1) for the first bending mode of a free–free beam ($x = 0.5L, \varepsilon = 0.001$). It should be noted that values of h_m and $h_{m\mathrm{HIGH}}$ will not correspond to those computed by using Eq. (13), since the graphics reflect the actual α for the location x but not the worst case estimate of α for a mode shape. Besides, the value of $\varphi''(x)$ at the utilized location x may not be equal to the value of M_{2L}.

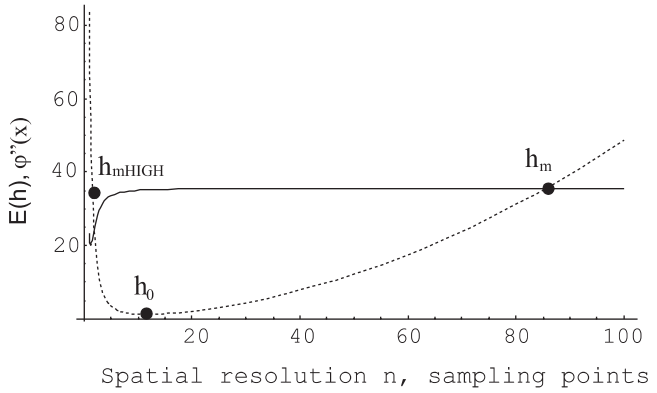

Fig. 6. $E(h)$ (dotted line) and noiseless $\varphi''(x)$ (solid line) for the first bending mode of a free–free beam; location $x = 0.5L$; noise level $\varepsilon = 0.001$.

3. Analysis of strain energy mode shapes

Strain energy mode shapes are usually computed by using the formula [9]

$$U_{ab} = \frac{1}{2}\int_a^b EI(\varphi'')^2\,\mathrm{d}x, \tag{15}$$

where U_{ab} is the strain energy calculated on the interval $a-b$; EI is the flexural stiffness of the cross section; $\varphi(x)$ is the mode shape vector (displacement mode shape); $\varphi''(x)$ is the modal curvature (curvature mode shape).

Thus, the optimal sampling interval for computing a strain energy mode shape should be closely related to that of the curvature mode shapes, as calculations of curvature play the central role in calculations of strain energy. Numerically, the computation of Eq. (15) is usually performed as follows: (1) taking the second derivative of a displacement mode shape as described in the previous section; (2) squaring of the curvature mode shape; (3) trapezoidal integration of the modal curvature (EI is assumed to be constant even for a damaged beam, and thus can be omitted).

Integration, performed in step 3 of the procedure above, will have the most significant impact on the optimal sampling interval for the strain energy mode shapes. Theoretically, the interval $a-b$ may include more than one sampling interval h. However, performing integration with $a-b>h$ does not seem necessary, as it will impede damage localization. It would be more practical to perform both differentiation and integration on the same interval $h = a-b$, which will provide the least errors in computation of the strain energy mode shapes.

The most commonly used, in damage detection, numerical formula for trapezoidal integration on an interval $a-b=h$ is [23]

$$\int_{x_0}^{x_0+h} f(x)\,\mathrm{d}x = \frac{h}{2}(f(x_0)+f(x_0+h)) - \frac{1}{12}h^3 f''(\xi_k) \quad \text{where } x_0<\xi_k<x_0+h. \tag{16}$$

The error term on the right represents the approximation error and is of $O(\mathrm{h}^3)$. The error diminishes with the reduction of h.

Denote $f(x) = (\varphi''(x))^2$, $\overline{f_0} = (\varphi''(x_0) + e_0)^2$, $\overline{f_1} = (\varphi''(x_0 + h) + e_1)^2$, $|e_i| \leqslant e$, where e_0 and e_1 are the errors of differentiation $E(h)$. Then the numerical formula for the strain energy value on the interval h is

$$U_h = \frac{1}{2}\left(\frac{h}{2}(\overline{f_0} + \overline{f_1}) - \frac{1}{12}h^3 f''(\xi_k)\right) = \frac{1}{2}\left(\frac{h}{2}((\varphi''(x_o))^2 + (\varphi''(x_o + h))^2) + E_I(h)\right),$$

where

$$E_I(h) = \frac{h}{2}(2e_0\varphi''(x_o) + e_0^2 + 2e_1\varphi''(x_o + h) + e_1^2) - \frac{1}{12}h^3 f''(\xi_k) \tag{17}$$

is the total error in the calculations of the strain energy. The $E_I(h)$ reflects the error due to noise in data, truncation error during differentiation, error from squaring, and approximation error during trapezoidal integration.

The maximum bound on $E_I(h)$ can be estimated as

$$|E_I| \leqslant eh(|\varphi''(x_o)| + |\varphi''(x_o + h)| + e) + \frac{M_2}{12}h^3, \tag{18}$$

where $M_2 = \max_{|x_0, x_0+h|}|((\varphi''(x))^2)''|$.

Analytical evaluation of Eq. (18) in an attempt to establish the optimal sampling interval h_0 is complicated and leads to solutions that are not easy to apply in practice. Instead, a numerical evaluation of Eq. (18) can be performed to connect the optimal sampling interval for curvature mode shapes to the optimal sampling interval for strain energy mode shapes. The goal of the numerical evaluation is to find $\min(E_I(h))\ \forall x$ and related h_0 for the given boundary conditions, measurement noise level ε, and mode number k, thus establishing the dependency between $h_{0\text{STRAIN}}$ and $h_{0\text{CURVATURE}}$ in the form

$$h_{0\text{STRAIN}} = g(h_{0\text{CURVATURE}}). \tag{19}$$

To perform the evaluation of the error behavior, both the error $E(h)$ for the curvature mode shapes and the error $E_I(h)$ for strain energy mode shapes were computed at every sampled location $x_i \in (0, L)$ along the beam length for a variety of spatial resolutions n_j and measurement noise levels ε. As an example, Fig. 7 shows the computational error $E(h)$ for curvature as a function of n_j and x_i for the second bending mode shape of a free–free beam with the noise level $\varepsilon = 0.01$ (1%). Fig. 8 illustrates the strain energy error $E_I(h)$ for the same beam. The optimal spatial resolution $n_{0\text{CURVATURE}} = 1/h_{0\text{CURVATURE}}$ for computation of the curvature mode shapes can be determined from the graph by finding a point $h_{0\text{CURVATURE}}$ such that $E(h_{0\text{CURVATURE}}) = \min(\max|E(h_j)\forall x_i|),\ j = [1, n_{\text{MAX}}], i = [1, j]$, where n_{MAX} is the maximal spatial resolution selected for the numerical experiment. The optimal spatial resolution $n_{0\text{STRAIN}} = 1/h_{0\text{STRAIN}}$ for computation of the strain energy mode shapes can be identified by finding a point $h_{0\text{STRAIN}}$ such that $E_I(h_{0\text{STRAIN}}) = \min(\max|E_I(h_j)\forall x_i|),\ j = [1, n_{\text{MAX}}], i = [1, j]$.

Utilizing the procedure described above, both $n_{0\text{CURVATURE}}$ and $n_{0\text{STRAIN}}$ were determined for several modes of beams with different boundary conditions and ε varying from 0.1 to 0.0000001. Then the value of $n_{0\text{STRAIN}}$ was plotted as a function of $n_{0\text{CURVATURE}}$ (Fig.9). The graph in Fig. 9 demonstrates a well-expressed linear dependency between the optimal sampling interval for the curvature and strain energy mode shapes. This dependency can be identified precisely by performing a linear regression on the dataset containing the combined data for all the boundary

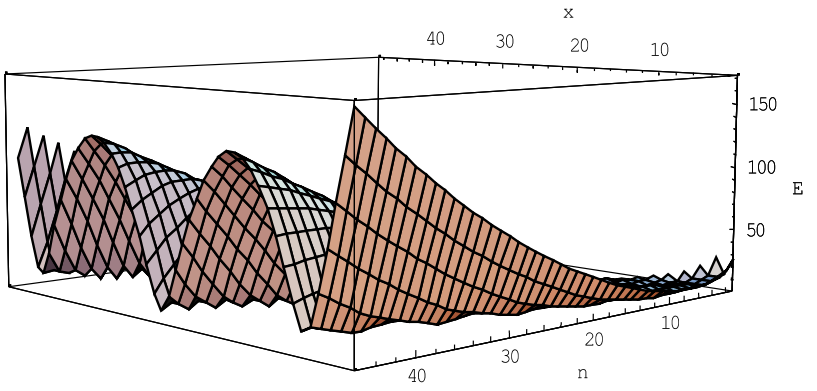

Fig. 7. Numerically computed $E(h)$ (curvature computation error) for the second mode of a free–free beam ($\varepsilon = 0.01$).

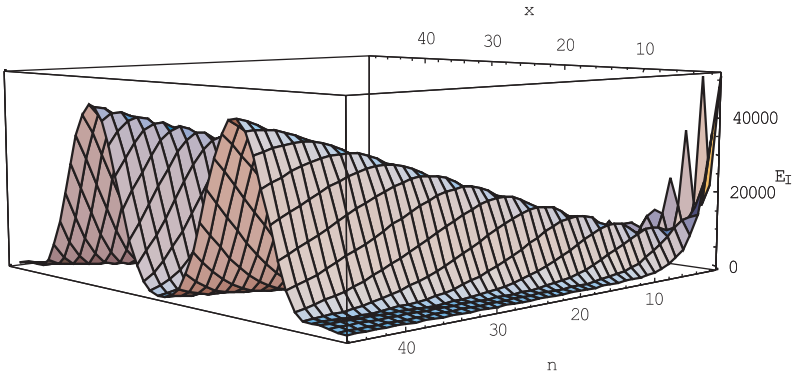

Fig. 8. Numerically computed $E_I(h)$ (strain energy calculation error) for the second mode of a free–free beam ($\varepsilon = 0.01$).

conditions and modes of vibration (Fig. 10). The linear regression produced the following dependency:

$$n_{0\mathrm{STRAIN}} = g_n(n_{0\mathrm{CURVATURE}}) = -1.83 + 1.327 n_{0\mathrm{CURVATURE}} = -1.83 + 1.327 \frac{1}{\sqrt[4]{\varepsilon F_4}}, \qquad (20)$$

with the correlation value of 0.9997 and standard deviation of 1.73. Or, in another form,

$$h_{0\mathrm{STRAIN}} = g_h(h_{0\mathrm{CURVATURE}}) = -0.00155 + 0.89 h_{0\mathrm{CURVATURE}} = -0.00155 + 0.89 \sqrt[4]{\varepsilon F_4}. \quad (21)$$

Formulas (20) and (21) can be used to calculate the optimal sampling interval for the computation of the strain energy mode shapes acquired with the relative measurement error ε. Both formulas utilize the optimal sampling interval for curvature mode shapes calculated by using formula (8b) as a basis for producing the value of $h_{0\mathrm{STRAIN}}$.

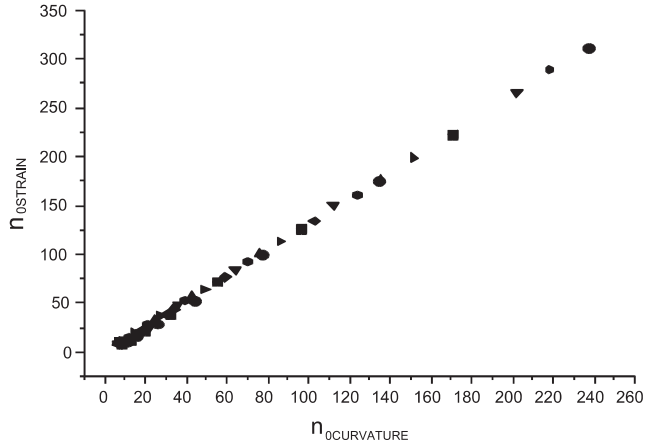

Fig. 9. Optimal spatial resolution for strain energy mode shapes as a function of optimal spatial resolution for curvature mode shapes: free–free, 2nd mode (■); free–free, 3rd mode (●); pinned–pinned, 2nd mode (▲); pinned–pinned, 3rd mode (▼); clamped–free, 2nd mode (◆); clamped–free, 3rd mode (◀); clamped–pinned, 2nd mode (▶); clamped–pinned, 3rd mode (●).

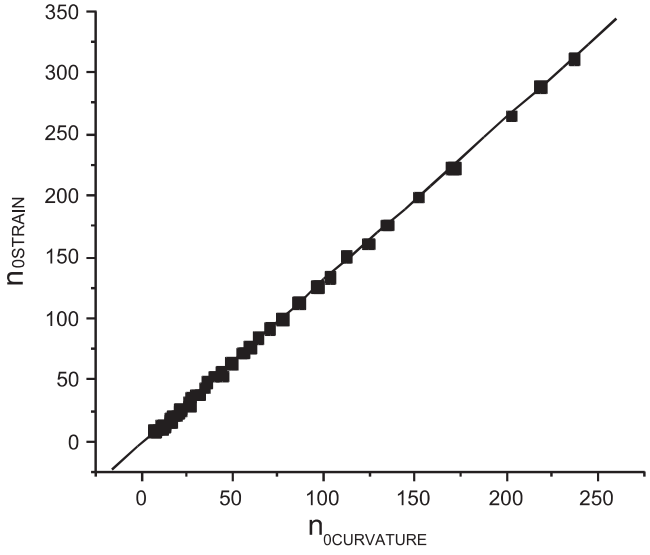

Fig. 10. Linear regression of the optimal sampling resolution of the strain energy mode shapes: combined data set (■); linear regression (solid line).

In the analysis of the curvature mode shapes, a limit value of h_m was established to estimate the minimum sampling interval, after which the computation of the curvature mode shapes begins to follow measurement noise rather than the mode shape function. For the computation of the strain energy mode shapes, the same limit h_m can be accepted as the minimal sampling interval

because computation of strain energy directly depends on the accuracy of the curvature calculations.

4. Effects of error distribution

Formulas for computing the optimal sampling interval for the curvature (8b) and the strain energy mode shapes (20) and (21) estimate the worst case scenario and do not account for error distribution within the interval $[-\varepsilon, \varepsilon]$. The probability of the largest measurement errors ε or $-\varepsilon$ occurring during an experiment depends upon the probability density function describing distribution of the measurement error. The probability of the worst case computational error in calculations of the curvature or the strain energy mode shapes is even smaller. For example, the occurrence of the worst case computational error for curvature mode shapes at location x requires the measurement error to take the value ε at location $x+h$, the value $-\varepsilon$ at location x and the value ε at location $x-h$ (assuming that the values of $\varphi_1, \varphi_0, \varphi_{-1}$ all have the same sign). As a result, the probability of the worst case computational error is less than the probability of the largest measurement error. This situation is illustrated in Figs. 11 and 12, which show the original uniform distribution of the measurement error ε_i and distribution of the computational error $E(h)$ for curvature mode shapes.

Because it is not guaranteed that the worst computational error will occur during a specific experiment, the formulas for the optimal sampling interval may seem to underpredict the value of h. The degree of underprediction depends upon the distribution of the measurement noise and the type of the function to be calculated (underprediction for calculations of the strain energy shapes is better expressed than for calculations of curvature). At the same time, formulas (8b), (20), and (21) guarantee the minimal computational error independently of noise distribution and specific measurement errors during an experiment and thus provide the most reliable estimate of h. If the goal is to find the optimal h for a different purpose (for example, such as to minimize the average computational error), the desired value of h may be obtained by accounting for the distribution of the measurement noise and computational errors, and correspondingly substituting the value of ε with the adjusted noise estimates.

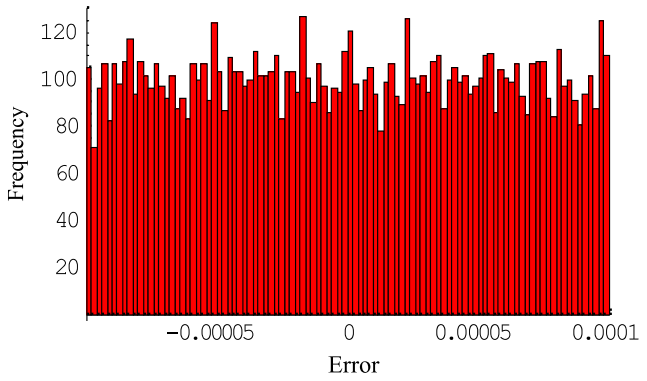

Fig. 11. Histogram of the uniformly distributed measurement error $|\varepsilon| \leqslant 0.0001$.

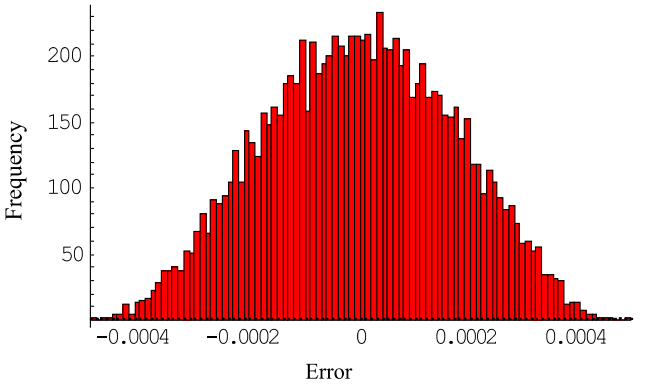

Fig. 12. Histogram of the computational error $E(h)$ for the curvature calculations (first mode of a free–free beam, $x = 0.5L, h = 0.1L$).

5. Numerical verification

Derivation of the formulas for the optimal sampling interval did not account for the changes due to damage in the beam. The motivation for such an analysis is that a less severe damage will cause very subtle changes in the displacement mode shapes, and thus does not influence the outcome. A more severe damage will cause visible changes in the displacement mode shapes, but the estimate of h for such a damage obtained through Eq. (8b) or (21) is a conservative one, i.e., a damaged displacement mode shape could be sampled at a higher resolution due to the fact that changes in the displacement mode shapes are going to be very significant around damaged locations. Thus, sampling the displacement mode shapes with the optimal sampling interval will produce the maximal sensitivity to small damages, while maximizing the resolution of damage localization (increasing the number of sampling points).

Normally, a damage detection procedure utilizing the curvature or the strain energy mode shapes requires acquisition of the displacement mode shapes from the undamaged structure and the structure under test (test mode shapes). For example, undamaged displacement mode shapes could be obtained from a knowingly good structure identical to the structure being tested or from historical data. After computation of curvature mode shapes, the undamaged curvature mode shapes are then subtracted from the curvature mode shapes for the test structure and the resulting "difference curvature mode shapes" are analyzed for peaks (indicators of damage). The same procedure applies to testing by strain energy mode shapes.

The performance of formulas (8b) and (21) was verified by evaluating the actual computational error in calculations of curvature and strain energy mode shapes. Error-free curvature and strain energy mode shapes were analytically computed from the displacement mode shape equations for a free–free beam. The same displacement mode shape equations were discretized for a number of sampling intervals with the number of sampling points varying from $n_{\min} = 4$ to $n_{\max} = 70$. Uniform noise was added to each sampling point. Curvature and strain energy mode shapes were numerically computed from the noisy data. The error at each sampling point was determined relative to the analytically computed values. The maximum computational error for each

sampling point was determined by repeating the procedure 10,000 times and selecting the maximal error from the obtained 10,000 values.

Fig. 13 shows the dependency of the relative computational error for curvature mode shapes of the first mode of a free–free beam on spatial resolution used for discretization of the displacement mode shapes. The measurement noise ε is 0.001%, and the error is computed at location $x = 0.5L$. The minimum of the computational error is observed for the spatial resolution $n = 10$; the optimal spatial resolution predicted by Eq. (8b) is also 10 sampling points.

Fig. 14 shows the dependency of the relative computational error for strain energy mode shapes for the same conditions. The minimum of the error is observed for spatial resolution $n = 14$; the optimal spatial resolution predicted by Eq. (21) is 12 sampling points.

Fig. 15 demonstrates the comparison of the numerically determined optimal spatial resolution for curvature mode shapes and the value predicted by formula (8b). Displacement mode shapes for a free–free beam were used in numerical computations. The values on the horizontal axis (''measurement noise'') are equivalent to 100ε. Fig. 16 shows the same comparison for strain energy mode shapes.

As indicated in Figs. 13–16, the optimal spatial resolution (determined in experiments with known *a priori* analytical solution for curvature and strain energy mode shapes) shows very good correlation to the results produced by formulas (8b), (20) and (21). Small differences in the prediction of the optimal spatial resolution of the strain energy mode shapes can be explained by the effect of the probability distribution that was discussed earlier. Overall, the suggested approach performed very well in determining the optimal sampling interval for the discretization of the displacement mode shapes (and subsequent computation of curvature or strain energy mode shapes).

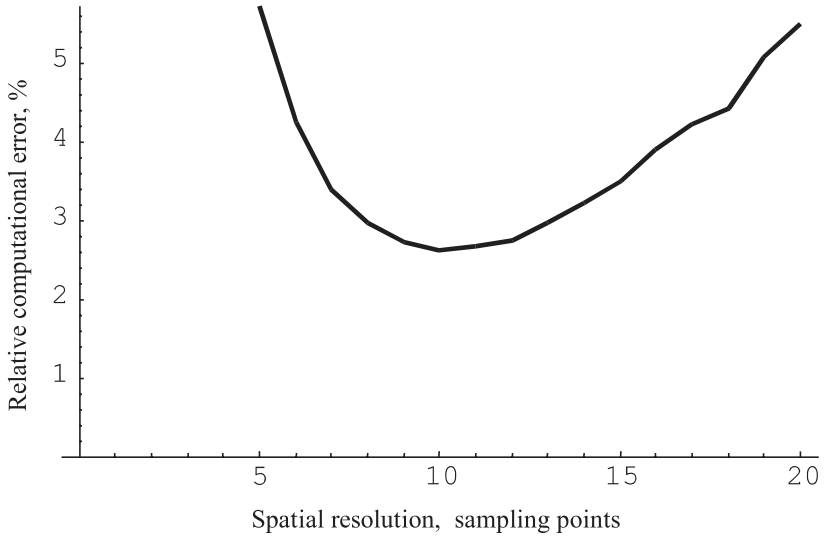

Fig. 13. Relative computational error for curvature mode shapes of the first mode of a free–free beam ($x = 0.5L$, $\varepsilon = 0.001$).

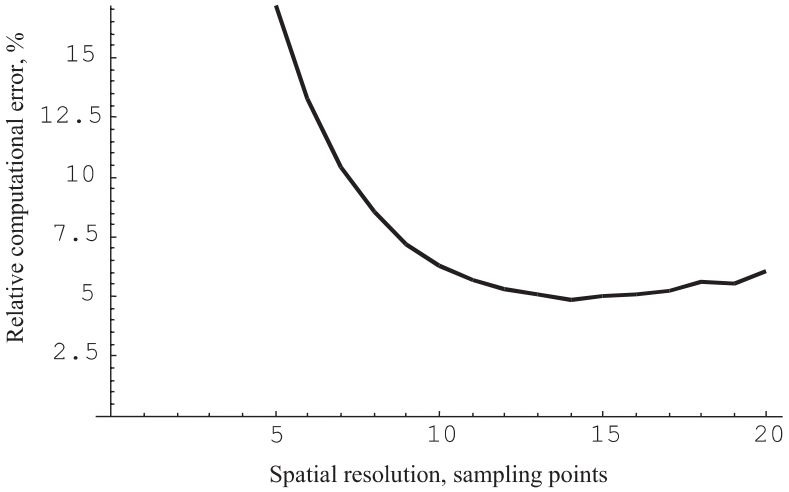

Fig. 14. Relative computational error for strain energy mode shapes of the first mode of a free–free beam ($x = 0.5L, \varepsilon = 0.001$).

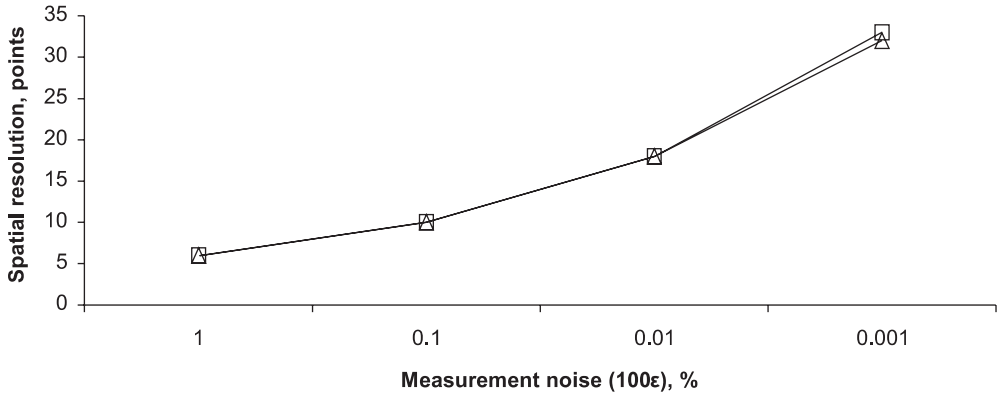

Fig. 15. Comparison of the numerically (□) and analytically (△) determined optimal spatial resolution for curvature mode shapes.

6. Conclusions

This paper attempted to address the practical issue of determining the optimal sampling interval for damage detection using strain energy mode shapes. The task was set on minimizing the effect of measurement noise in commonly used numerical methods, while providing maximum sensitivity to damage and maximizing the spatial resolution. The suggested approach identifies the optimal sampling interval to be used for acquisition of the displacement mode shapes. Utilizing the optimal sampling interval may be especially important for the recent data acquisition methods capable of very dense sampling, such as laser vibrometry. Application of a laser vibrometer for the goal of better damage localization though denser sampling may have adverse effects on the quality of damage detection if no special care is taken to reduce measurement noise.

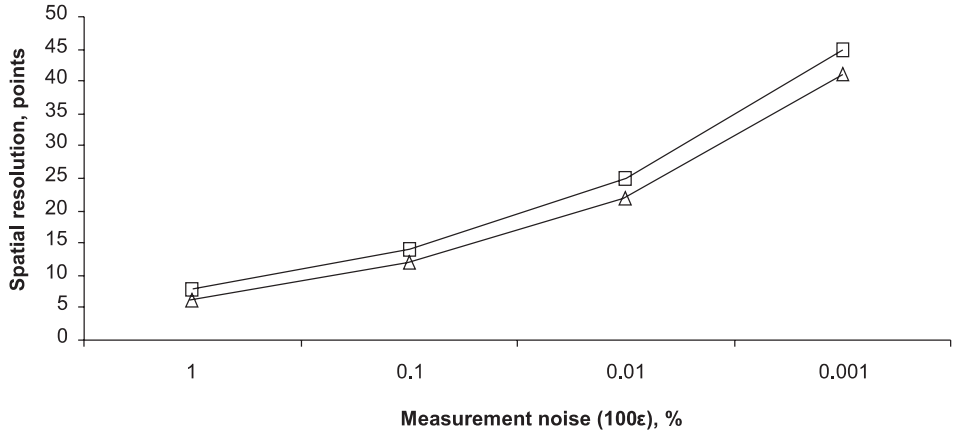

Fig. 16. Comparison of the numerically (□) and analytically (△) determined optimal spatial resolution for strain energy mode shapes.

Formulas (8b), (20), and (21) should be used to estimate the optimal sampling interval for the acquisition of the displacement mode shapes and subsequent calculation of curvature or strain energy mode shapes. Table 1 lists the parameters that can be applied in practical calculations of spatial resolution for the most commonly used boundary conditions of a beam. Applied with the parameters from Table 2, formula (14) can be utilized to determine the maximum number of sampling points, after which the measurement noise begins to dominate the results of calculations and the calculated curvature or strain energy mode shapes become meaningless. Numerical verification of the suggested formulas showed very good performance of the method in predicting the optimal sampling interval.

Practical determination of the optimal spatial sampling interval requires correct estimates of measurement error ε, which is dependent on utilized measurement equipment and testing methodology. In general, statistical methods can be applied to produce estimates of ε for each particular experimental setup.

References

[1] A.K. Pandey, M. Biswas, M.M. Samman, Damage detection from changes in curvature mode shapes, *Journal of Sound and Vibration* 145 (1991) 321–332.

[2] C.P. Ratcliffe, Damage detection using a modified Laplacian operator on mode shape data, *Journal of Sound and Vibration* 204 (1997) 505–517.

[3] B. Hoerst, C.P. Ratcliff, Damage detection in beams using Laplacian operators on experimental modal data, in: *Proceedings of International Modal Analysis Conference (IMAC-XV)*, Orlando, FL, 1997, pp. 1305–1311.

[4] C.R. Farrar, D.A. Jauregui, Comparative study of damage identification algorithms applied to a bridge, *Smart Materials and Structures* 7 (1998) 704–719.

[5] Q. Lu, G. Ren, C. Zhao, Multiple damage location with flexibility curvature and relative frequency change for beam structures, *Journal of Sound and Vibration* 253 (2002) 1101–1114.

[6] R.P.C. Sampaio, Damage detection using the frequency response function curvature method, *Journal of Sound and Vibration* 226 (1999) 1029–1042.

[7] A. Dutta, S. Talukdar, Damage detection in bridges using accurate modal parameters, *Finite Elements in Analysis and Design*, 2003.
[8] S.H. Petro, S. En, H. GangaRao, S. Venkatappa, Damage detection using vibration measurement, in: *Proceedings of International Modal Analysis Conference (IMAC-XV)*, Orlando, FL, 1997, pp. 113–119.
[9] S.G. Venkatappa, Damage Detection using Vibration Measurements, Master of Science Thesis, West Virginia University, 1997.
[10] R.A. Osegueda, C.J. Carrasco, R. Meza, A modal strain energy distribution method to localize and quantify damage, in: *Proceedings of International Modal Analysis Conference (IMAC-XV)*, Orlando, FL, 1997, pp. 1298–1304.
[11] C. Carrasco, R. Osegueda, C. Ferregut, M. Grygier, Damage localization in a space truss model using modal strain energy, in: *Proceedings of International Modal Analysis Conference (IMAC-XV)*, Orlando, FL, 1997, pp. 1786–1792.
[12] P. Cornwell, M. Kam, B. Carlson, B. Hoerst, S. Doebling, C. Farrar, Comparative study of vibration-based damage ID algorithms, in: *Proceedings of International Modal Analysis Conference (IMAC-XVI)*, Santa Barbara, CA, 1998, pp. 1710–1716.
[13] A. Wahab, G. Roeck, Damage detection in bridges using modal curvatures: application to a real damage scenario, *Journal of Sound and Vibration* 226 (1999) 217–235.
[14] S.H. Yoo, H.K. Kwak, B.S. Kim, Detection and location of a crack in a plate using modal analysis, in: *Proceedings of International Modal Analysis Conference (IMAC-XVII)*, Orlando, FL, 1999, pp. 1902–1908.
[15] L. Pereyra, R. Osegueda, C. Carrasco, C. Ferregut, Detection of damage in a stiffened plate from fusion of modal strain energy differences, in: *Proceedings of International Modal Analysis Conference (IMAC-XVIII)*, San Antonio, TX, 2000, pp. 1556–1562.
[16] P. Cornwell, S. Doebling, C. Farrar, Application of the strain energy damage detection method to plate-like structures, *Journal of Sound and Vibration* 224 (1999) 359–374.
[17] J.M. Ndambi, J. Vantomme, K. Harri, Damage assessment in reinforced concrete beams using eigenfrequencies and mode shape derivatives, *Engineering Structures* 24 (2002) 501–515.
[18] J.T. Kim, Y.S. Ryu, H.M. Cho, N. Stubbs, Damage identification in beam-type structures: frequency-based method vs mode-shape-based method, *Engineering Structures* 25 (2003) 57–67.
[19] K. Napolitano, Damage detection using reduced measurements: analytical investigation, http://casl.ucsd.edu/casl/abstracts/abstract_damage_detect_ai.htm.
[20] Z.Y. Shi, S.S. Law, Structural damage localization from modal strain energy change, *Journal of Sound and Vibration* 218 (1998) 825–844.
[21] S.H. Yoo, B.S. Kim, Characterization of a crack in a plate using strain mode shapes, in: *Proceedings of International Modal Analysis Conference (IMAC-XVIII)*, San Antonio, TX, pp. 1790–1795.
[22] P. Yan, Y. Deng, Nondestructive damage detection of bridges based on strain mode, in: *Proceedings of International Modal Analysis Conference (IMAC-XVIII)*, San Antonio, TX, 2000, pp. 1825–1830.
[23] W. Gautschi, *Numerical Analysis. An Introduction*, Purdue University, Indiana, 1997.
[24] R.W. Southworth, S.L. Deleeuw, *Digital Computation and Numerical Methods*, McGraw-Hill, New York, 1965.
[25] R. Blevins, *Formulas for Natural Frequency and Mode Shape*, Krieger, Melbourne, FL, 2001.